SPACE-DEPLOYABLE REFLECTARRAY ANTENNA IN L-BAND

M.Tech. Thesis

By

SREYA GHOSH

DEPARTMENT OF ASTRONOMY, ASTROPHYSICS AND SPACE ENGINEERING

INDIAN INSTITUTE OF TECHNOLOGY INDORE

May 2025

SPACE-DEPLOYABLE REFLECTARRAY ANTENNA IN L-BAND

A Thesis

Submitted in partial fulfillment of the
requirements for the award of the degree
of
Master of Technology

by

SREYA GHOSH

DEPARTMENT OF ASTRONOMY, ASTROPHYSICS AND SPACE ENGINEERING

INDIAN INSTITUTE OF TECHNOLOGY INDORE

May 2025

INDIAN INSTITUTE OF TECHNOLOGY INDORE

CANDIDATE'S DECLARATION

I hereby certify that the work which is being presented in the thesis entitled **SPACE-DEPLOYABLE REFLECTARRAY ANTENNA IN L-BAND** in the partial fulfillment of the requirements for the award of the degree of **MASTER OF TECHNOLOGY** and submitted in the **DEPARTMENT OF ASTRONOMY, ASTROPHYSICS AND SPACE ENGINEERING, Indian Institute of Technology Indore**, is an authentic record of my own work carried out during the time period from July 2023 to May 2025 under the supervision of Dr. Abhirup Datta, Professor, Department of Astronomy, Astrophysics and Space Engineering, IIT Indore.

The matter presented in this thesis has not been submitted by me for the award of any other degree of this or any other institute.

Sreya Ghosh 16.05.2025

Signature of the student with date

(SREYA GHOSH)

This is to certify that the above statement made by the candidate is correct to the best of my/our knowledge.

16.05.2025

Signature of the Supervisor with date

(Dr. ABHIRUP DATTA, PROFESSOR)

SREYA GHOSH has successfully given his/her M.Tech. Oral Examination held on **6th May, 2025**.

16.05.2025

Signature(s) of Supervisor(s)

Date:

Programme Coordinator, M.Tech.

Date: 16-05-2025

Manoneeta Chakraborty

Convenor, DPGC

Date: 16/05/2025

HoD, DAASE

Date:

ACKNOWLEDGEMENTS

I would like to express my sincere gratitude to my thesis supervisor, Prof. Abhirup Datta, for his support and guidance throughout the course of this research work. I am also thankful to the faculty and staff of the Department of Astronomy, Astrophysics and Space Engineering, IIT Indore, for their support and for providing the infrastructure and facilities essential for carrying out this research work.

I am indebted to Dr. Saptarshi Ghosh, Associate Professor of Electrical Engineering Department of IIT Indore, for his invaluable guidance, and his PhD student Mr. Akhila Gowda for his sincere assistance.

I extend my profound gratitude to Dr. Rinkee Chopra, Assistant Professor of Electrical Engineering Department of IIT Indore, for her indispensable guidance and contributions.

I thank my parents for their unconditional love, patience and understanding. Their constant support has been the foundation of all my efforts. Lastly, I am obliged to have received the constant help and support of my friend and classmate that have been a beacon in the journey of this research work.

Abstract

This thesis introduces a novel space-deployable reflectarray(RA) antenna in L band (1-2 GHz) tailored to be stowed in CubeSats. The lower frequency of L band makes the size of reflectarray considerably large to be stowed in microsatellites. The novel design aims to incorporate miniaturization of the phasing elements of the reflectarray to diminish the overall size of the structure. The RA is made up of 256 unit cells, each of periodicity 35mm and a third order Minkowski fractal. The feed antenna designed for the RA system is a 2×2 patch array. The patch array and the RA together make the RA system compact and easy to be deployed in a CubeSat. This work aims to contribute to space-deployable compact L band antennas for better understanding of the universe's structure and evolution.

A precursor to space deployment of the reflectarray antenna can be a deployment of the antenna for RFI survey in the pristine radio-silent Arctic region. Radio frequency interference (RFI) is a crucial aspect of radio astronomy. Thus the thesis presents the preliminary results of the RFI survey conducted at the Himadri Station in Svalbard, Arctic. The frequency range of 100 kHz to 1750 MHz is significant for various low-frequency radio astronomy studies, such as redshifted 21 cm observations. This work examines the potential of Himadri Station as a suitable site for RFI-free radio astronomy observations. The experiment provides a hands-on experience of the use of antennas for radio astronomical purposes.

LIST OF PUBLICATIONS

1. Sreya Ghosh, Harsha Avinash Tanti, Abhirup Datta and Saurabh Das, “AN OVERVIEW OF ARCTIC RFI MONITORING SURVEY,” accepted in *2024 IEEE India Geoscience and Remote Sensing Symposium (InGARSS)*.

Contents

List of Figures

List of Tables

ACRONYMS

RA	**Reflectarray**
FPR	**Folded Panel Reflectarray**
RFI	**Radio Frequency Interference**
ISARA	**Integrated Solar Array and Reflectarray**
VLBI	**Very Long Baseline Interferometry**
AVA	**Antipodal Vivaldi Antenna**

Chapter 1

Introduction

1.1 Fundamentals of Reflectarrays

The IEEE Standard for Definitions on Terms for Antennas [25], designates a reflectarray as: "An antenna consisting of a feed and an array of reflecting elements arranged on a surface and adjusted so that the reflected waves from the individual elements combine to produce a prescribed secondary radiation pattern". A reflectarray antenna [25] is of a planar or conformal array of elements that are excited with a feed antenna as in the Figure 1.1. When illuminated by the feed antenna, each element produces a certain reflected phase. The phase distribution across the reflectarray aperture is designed to create a collimated or shaped beam in the desired direction. Designing a reflectarray involves two main steps, namely, element design and system design.

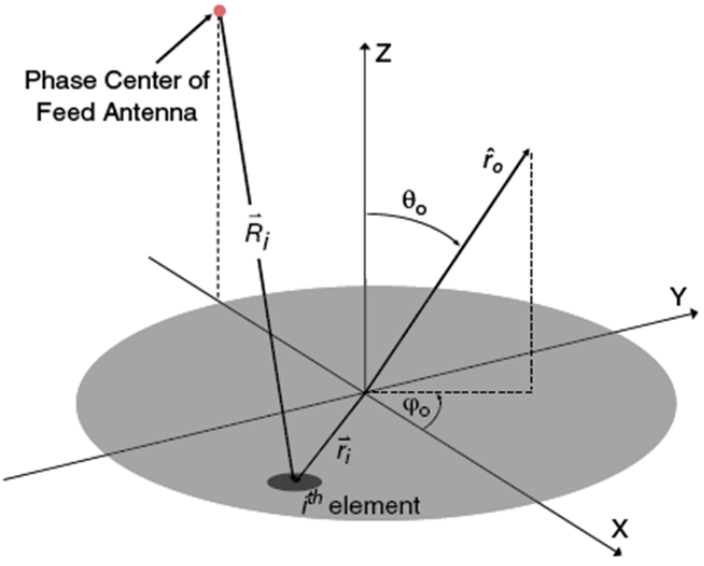

Figure 1.1: Reflectarray with feed antenna

In classic planar antenna arrays, a uniform phase distribution on the aperture will yield a collimated beam in the broadside direction, i.e., normal to the plane of the array. To steer the beam in a specific direction, a progressive phase distribution is assigned to the array elements. Reflectarrays operate on the same principle, but the position of the feed antenna must also be considered. The feed antenna is positioned relative to the reflectarray's coordinate system, as shown in the figure.

The reflectarray elements are typically assumed to be in the feed antenna's far field, allowing the incident electromagnetic field on each element to be approximated as a plane wave with a specific incident angle. The electromagnetic fields radiating from the feed propagate as a spherical wave originating from the phase center of the feed antenna. The incident fields on the reflectarray aperture exhibit a phase delay proportional to the distance traveled, referred to as the spatial phase delay. The reflection phase of a reflectarray element must compensate for the spatial phase delay (SPD) from the feed phase center to that element to form a collimated beam. Mathematically, this is expressed as:

$$\phi_{\text{spd}} = -k_0 R_i, \tag{1.1}$$

where R_i, k_0 are the distance from the feed phase center to the ith element, and the wavenumber at the center frequency respectively. Such a phase distribution converts the spherical wave radiated by the feed antenna into a collimated beam in the broadside direction (the Z-direction relative to the Figure 1.1). To scan this collimated beam in any other direction, a progressive phase (PP) can be added to the aperture, which in vector form is given by:

$$\phi_{\text{pp}} = -k_0 \vec{r}_i \cdot \hat{r}_0, \tag{1.2}$$

where $\vec{r}_i$, $\hat{r}_0$ are the position vector of the ith element, and the direction of the main beam respectively, as shown in Figure 1.1. In the Cartesian coordinate system of the figure, the position of each element can be expressed as (x_i, y_i). Thus, for a beam directed in a certain spherical direction (θ_0, ϕ_0), this equation is:

$$\phi_{\text{pp}} = -k_0 \left(x_i \sin\theta_0 \cos\phi_0 + y_i \sin\theta_0 \sin\phi_0 \right). \tag{1.3}$$

The required phase shift on the reflectarray aperture must compensate for the spatial delay ($-\phi_{\text{spd}}$) and add the progressive phase to the aperture. This is given by:

$$\phi_{\text{total}} = k_0 \left(R_i - \sin\theta_0 \left(x_i \cos\phi_0 + y_i \sin\phi_0 \right) \right) + \phi_0, \tag{1.4}$$

where ϕ_0 is a phase constant, indicating that a relative phase is needed for the reflectarray elements. The required phase distribution given in Equation (1.4) will produce a pencil beam in the desired direction.

1.2 Reflectarray For Space-Borne Applications

A **Reflectarray (RA)** is a type of antenna that combines the features of a traditional reflector (like a parabolic dish) and a phased array. Compared to conventional antenna designs and parabolic reflectors, RAs offer the following advantages:

1. **Low Weight and Compact Design:** Reflectarrays are lightweight and have a low profile compared to traditional parabolic reflectors, making them suitable for launch and deployment in space, where weight and size are critical factors.

2. **High Beam-Steering Capability:** By electronically controlling the phase of individual elements, reflectarrays can steer beams without mechanical movement, offering flexibility in pointing and tracking targets in dynamic space environments.

3. **Ease of Manufacturing:** Reflectarrays are simpler to manufacture than conventional curved reflectors, as they use flat or slightly curved surfaces. This reduces production complexity and cost, which is beneficial for space missions.

4. **Scalability:** The planar structure of reflectarrays makes them highly scalable, allowing for the design of large apertures necessary for high-gain communication systems.

5. **Reduced Structural Complexity:** Unlike traditional reflector antennas, reflectarrays do not require large and mechanically complex support structures, which simplifies integration and deployment in space.

6. **High Efficiency:** Reflectarrays can achieve high radiation efficiency by minimizing feed blockage and tailoring phase corrections to compensate for spatial phase delays and feed distortions.

7. **Adaptability to Conformal Surfaces:** Reflectarrays can be designed to conform to spacecraft surfaces, optimizing the use of available space and enabling innovative antenna designs.

1.3 Literature Review

Reflectarrays have gained more popularity than the phased arrays and parabolic reflector antennas due to their advantages namely ease of manufacture in flat panels, low losses, low cross polarization, and electronic beam control. The paper [1] reviews the different contributions in reflectarrays from fixed-beam to reconfigurable-beam implementations in single and multilayer configurations. This includes applications for linear and circular polarization, single and multiple beams, pencil and shaped beams, and also discusses single and dual reflectarray configurations. The paper [2] reviews the design and experimental features of reflectarray antennas for bandwidth improvement in microwave and millimeterwave frequency ranges.

In [3] inflatable array antennas are studied which were being developed to reduce the mass, stowage volume, and cost of future spacecraft systems. Earth remote-sensing and deep-space-exploration programs have increasing demands for high-gain and large-aperture antennas on spacecraft. To meet these goals, large-aperture antennas must be deployable. An inflatable parabolic reflector was introduced as deployable about two decades ago. However, the full implementation of this concept is still hampered by the inability to achieve and maintain the required surface accuracy. To mitigate the problem associated with curved surfaces, a new class of planar-array technology has been developed. However, membrane flatness and separation are crucial for maintaining required aperture efficiency and sidelobe/cross-pol levels. The required membrane separation tolerance should be smaller than 1/20th of the absolute separation distance.

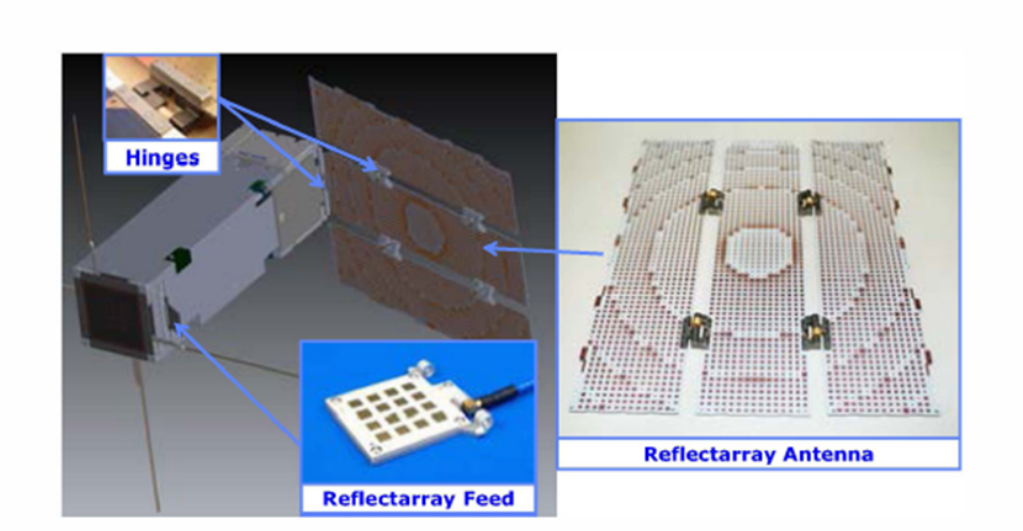

Figure 1.2: CubeSat deployable Reflectarray in ISARA[4]

In [4], two novel high gain deployable reflectarray antennas are described and compared with other high gain CubeSat antenna technologies. Figure 1.2 shows the 3-panelled reflectarray in ISARA. The folded panel reflectarrays can have 3-6 panels. Scalability being the main limitation, the number of panels is restricted due to the following factors: (1) tolerance accumulation of multiple hinged panels limits the size of a practical FPR, and (2) there is a practical limit to how thin one can make a panel and still meet flatness requirements, so stacking a large number of panels will consume CubeSat payload volume.

The paper [5] discusses the design of an L-band circularly polarized reflectarray antenna for BeiDou satellite applications. The antenna is designed using variable-sized microstrip patch elements with a double-layer substrate to minimize dielectric loss, antenna weight, and system cost. However the size and the reflectarray being dual-layered makes its deployability difficult.

[7]-[12] studies the different shapes for the reflecting elements and its effects on the printed reflectarray. [13], [14] studies miniaturization of the patch elements for lower frequencies using fractals. In [14], the paper presents a Minkowski fractal-shaped patch for the design of a reduced-size reflectarray element. The intrinsic miniaturization capability of the fractal geometry is fully exploited by leaving unchanged the patch length and using the fractal scaling factor to obtain a good reflectarray phase agility. This size reduction effect allows for the choice of array grids with smaller interelemental spacing. A fractal-shaped X-band reflectarray element, embedded into a cell, is designed to give a high phase agility range, greater than 300˚. This technique can be adopted to minimize the patch element size for L-band as well and thus, reduce the overall dimensions of the reflectarray.

1.4 Importance of L Band

The L-band (1–2 GHz) is vital for radio astronomy for several reasons. It encompasses the 21 cm spectral line (1.42 GHz), which is emitted by neutral hydrogen (HI). This line is essential for studying the structure, dynamics, and distribution of hydrogen in the universe, helping astronomers in mapping galaxies and investigating the large-scale structure of the cosmos. Many pulsars emit strongly in the L-band, making it crucial for their detection and analysis. L-band observations also play a key role in tracing cosmic evolution by mapping neutral hydrogen at various redshifts, offering insights into galaxy formation and the distribution of dark matter. Furthermore, the L-band is excellent for observing extended structures like galactic disks and gas clouds, providing

valuable information about star formation and the interstellar medium.

Earth's atmosphere can significantly distort and absorb radio waves in the L-band. Ionospheric scintillations and perturbations affect the propagation of radio waves. Thus a space-based L-band antenna can continuously survey the sky, uninterrupted by atmospheric phenomena as well the day-night cycle. The L-band is widely used for communication and radar systems, leading to significant interference when using ground-based telescopes in this frequency range. Thus space-based L-band antenna can provide less distorted data and more reliable observations. Space-based L-band observations enable the detection of low-frequency signals that are otherwise blocked by Earth's atmosphere, such as emissions from distant galaxies, cosmic microwave background (CMB) studies, and large-scale structures in the universe. This opens up new avenues for exploring the early universe and cosmology.

1.5 Research Gap

In CubeSat applications, minimizing payload volume is crucial. Although reflectarray antennas operating at different frequencies have been developed in previous research, only a limited number of L-band reflectarray antennas have been suggested for high-gain purposes [5, 6]. At lower frequencies like L-band, the antenna size becomes large resulting in lower aperture efficiency. Miniaturization of the unit cells is, thus, needed to reduce the overall size of the antenna [13, 14]. Currently most space-borne antennas are not suitable for CubeSat applications due to their size and stowage volume [5,6]. L-band antennas are crucial in radio astronomy for observing a range of celestial phenomena, including the study of pulsars, galaxies, and cosmic microwave background radiation. In the context of radio astronomy, L-band typically refers to frequencies in the range of 1 to 2 GHz. These frequencies are used for both ground-based and space-based observatories, enabling the detection of various cosmic signals. Space-based radio telescopes also use L-band for communication and scientific observation. The Parker Solar Probe and other solar observatories use L-band to study the Sun and space weather. Space-based observatories such as the RadioAstron mission (which used a space-based antenna in conjunction with ground stations) utilized L-band for high-resolution imaging of distant galaxies and cosmic objects. A 2-element CubeSat-based radio interferometer prototype, operating at 1.4 GHz with a microstrip square patch antenna, was developed in our lab. To push this system towards space VLBI (Very Long Baseline Interferometry), which connects antennas over vast distances for better angular resolution, the microstrip antenna

can be replaced by a high-gain, space-deployable reflectarray antenna for enhanced performance.

1.6 Problem Statement

The thesis presents a novel design of the reflectarray with high-gain and compactness for CubeSats applications. The design seeks to integrate a miniaturized reflectarray together with a compact feed antenna to keep the system lightweight. Miniaturization of the unit cells will provide overall reduction in size of the reflectarray, thus facilitating foldability with reduced stowage volume. The compact feed antenna will make the system easy to be deployed in a CubeSat. The design thus presents the novel concept of high-gain, compact reflectarray system for use in CubeSats, operating in the L-band to observe a range of celestial phenomena.

1.7 Organization of The Thesis

The thesis is organized in the following manner: first the design of reflectarray is discussed in detail along with the results in Chapter 2. In chapter 3 the Arctic RFI Survey is presented along with results and the discussions in Chapter 3. Finally, chapter 4 discusses the conclusion and scope for future work.

Chapter 2

Design of Reflectarray

2.1 Design of Unit Cell

In [14] miniaturization using fractals has been studied. The phase of S_{11} for varying the size of patches for different shapes have been investigated as shown in Figure 2.1. The studied geometries are the first iteration of Koch-triangle, Minkowski, and Koch-square.

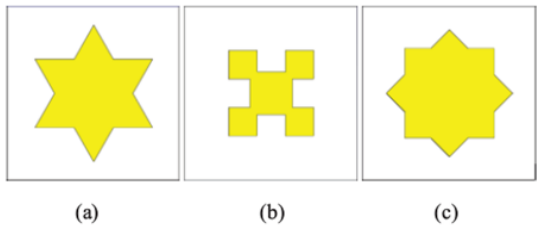

Figure 1: (a) Koch-triangle. (b) Minkowski. (c) Koch-square.

(a) Koch-triangle, Minkowski, and Koch-square

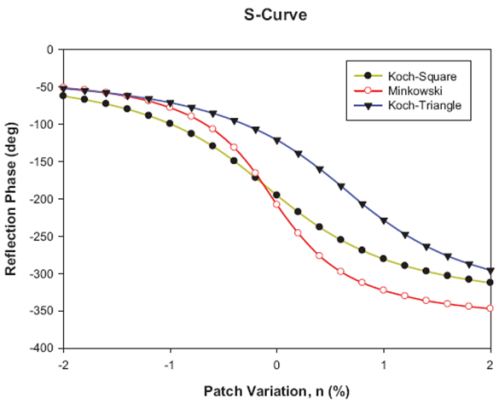

(b) Patch variation vs Reflection phase.

Figure 2.1: Reflection phase study of first iteration of various fractals [14]

The S_{11} results show that the Minkowski fractal has the highest linear phase range (300˚). Thus the Minkowski fractal reflecting element same has been replicated using CST studio 2019. A single layer unit cell of reflectarray has been simulated. A block of unit cell reflectarray is modelled as in Figure 2.3 and parameters such as permittivity which is dielectric constant, substrate and copper thickness, tangential loss and geometry of radiating element are defined. The substrate used has relative permittivity of 3.54 and thickness (t) of 1.524 mm. Copper thickness considered is 0.035 mm. The periodicity of the unit cell is 11.43×10.16 (all in mm). The patch length of the fractal has

been varied as shown in Figure 2.4. After simulation, the S_{11} phase variation shown in Figure 2.2 is found to be similar as in [14].

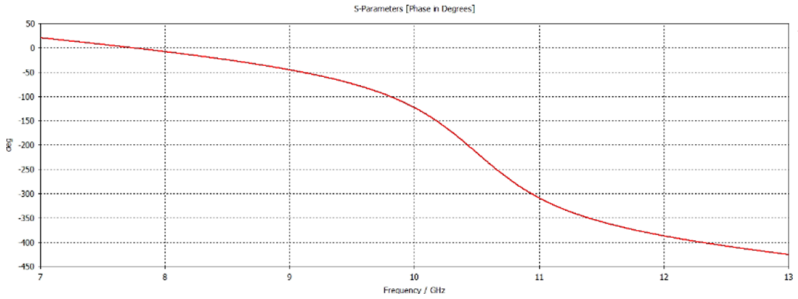

Figure 2.2: Simulation result of the reflection phase of the replicated Minkowski fractal patch

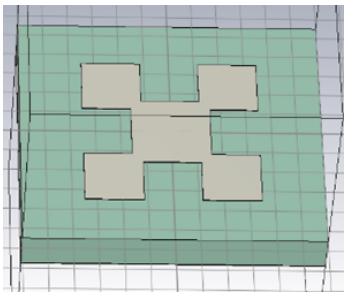

(a) Minkowski fractal patch in X-band.

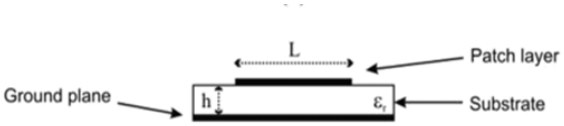

(b) Configuration of substrate, patch layer, and ground plane.

Figure 2.3: Minkowski fractal patch and configuration details.

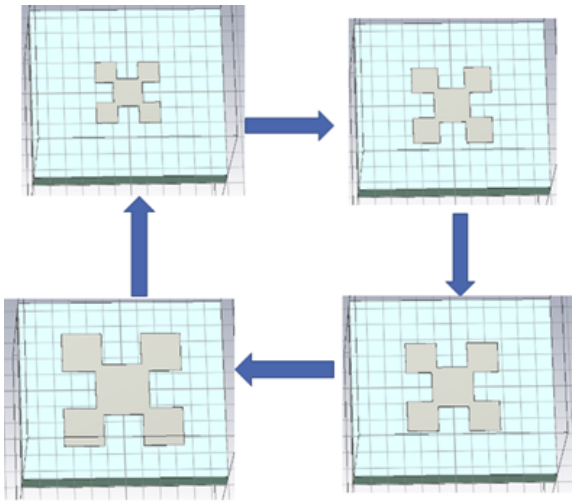

Figure 2.4: Variation of the Minkowski patch for increasing patch length.

Next, the substrate has been replaced with FR4 substrate with dimensions 11×12×1.524 (all dimensions are in mm). The patch size is varied from 4-7mm.

The patch dimension was varied to obtain the phase response of S_{11}.

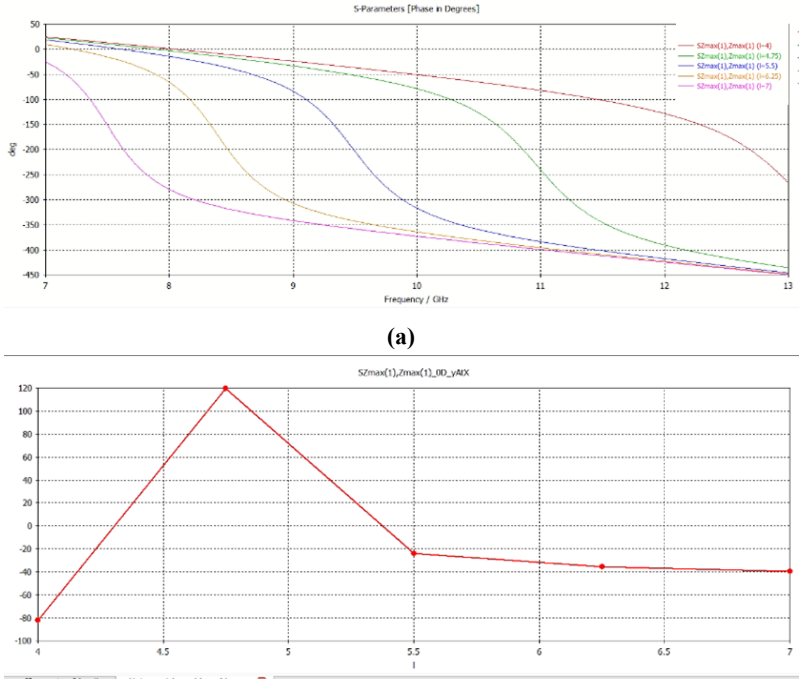

(a)

(b)

Figure 2.5: Phase of S_{11} for different patch lengths (in mm) at frequency = 11 GHz.

At 11 GHz, the Figure 2.5 shows that the phase of S_{11} changes from $-80°$ to $+120°$ as the patch length increases. Thus, a total phase change of $200°$ is achieved at the X-band. Additionally, the phase change is linear with an increase in the patch length.

The fractal and the unit cell are next scaled for 2-6 GHz as in Figure 2.6. The periodicity is 24mm. The patch size is varied from 8-16mm to get the phase variation of S_{11} as seen in Figure 2.7.

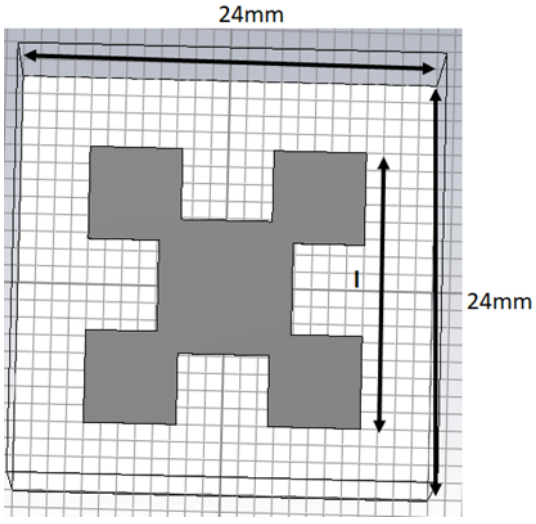

Figure 2.6: First iteration of Minkowski square fractal

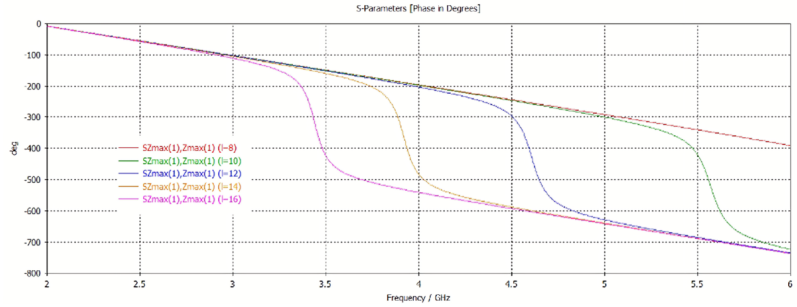

Figure 2.7: Phase of S_{11} for different patch lengths (in mm) at frequency = 4 GHz.

In [13] lowering the resonating frequency is achieved by a fixed size patch only by increasing the iteration order of the Minkowski fractal. The fractal reflectarray element uses the Minkowski geometry as Figure 2.8. A square element generator of dimensions L × L (Figure 2.8a) is iteratively modified as follows. In the first iteration a smaller square of side SL is removed from the center of each generator patch side (Figure 2.8b), giving the fractal scaling factor varying from 0 up to L/3. When applying the above operation to each side of the first-order fractal structure, the second iteration patch is obtained (Figure 2.8c). The fractal generation can then, be infinitely reiterated to obtain an increasingly complex self-similar shape. The phase of S_{11} in Figure 2.9 shows that increasing the order of iteration lowers the operating frequency.

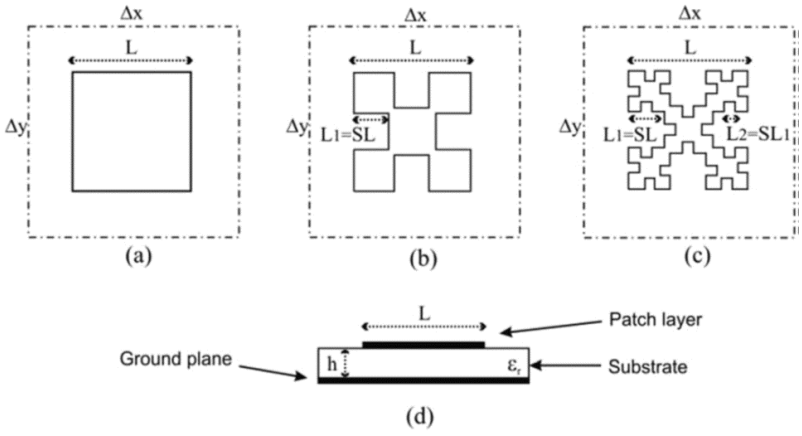

Figure 2.8: Minkowski fractal patch: (a) square patch generator; (b) first-iteration patch; (c) second-iteration patch; (d) antenna layers [13]

Accordingly, 2nd iteration of the fractal is used for 2-4 GHz as illustrated in Figure 2.10 to utilize the miniaturization effect of the fractal geometry. The periodicity is same as in the 2-6 GHz unit cell, which is 24mm. However, the overall patch size now varies from 17-23mm to achieve phase tuning shown in Figure 2.11.

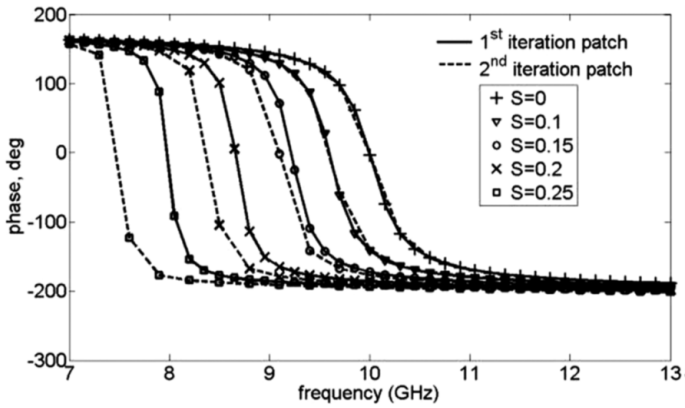

Figure 2.9: Phase of S_{11} vs frequency first and second iteration of the Minkowski patch [13]

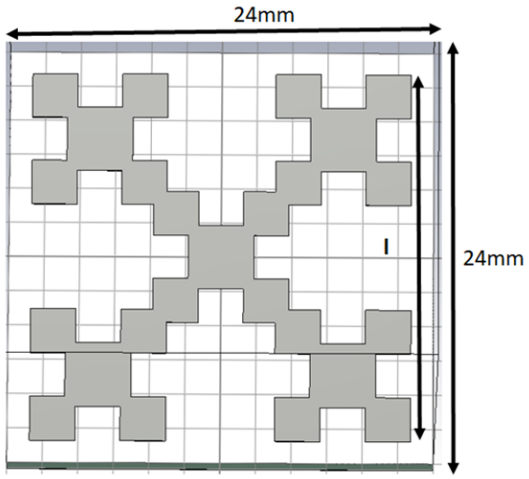

Figure 2.10: Second iteration of Minkowski fractal

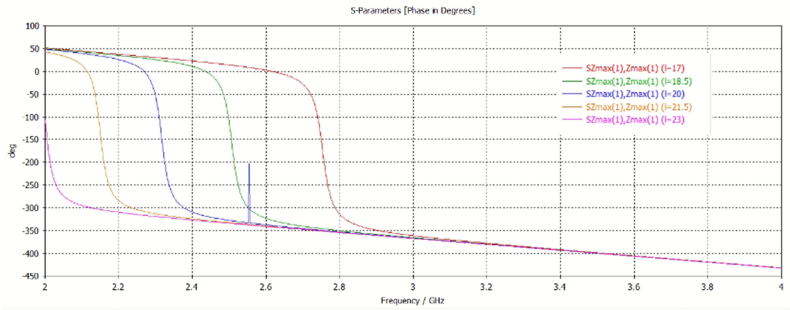

Figure 2.11: Phase of S_{11} for different patch lengths (in mm) at frequency = 2.5 GHz.

Next, 3rd iteration of the fractal is used for 1-2 GHz illustrated in Figure 2.12. The patch size and the periodicity are optimized. The periodicity is 35mm. The patch length varies from 25-30mm to get a phase range of $0°$ to $180°$ as shown in Figure 2.13. Thus phase tuning is achieved as well as miniaturization technique is utilized to reduce the inter-elemental spacing and the overall dimension of the reflectarray. Dr. Saptarshi Ghosh, Associate Professor in the Electrical Engineering Department, IIT Indore, has assisted in the incorporation of the concept of the fractals in unit cells

for miniaturization.

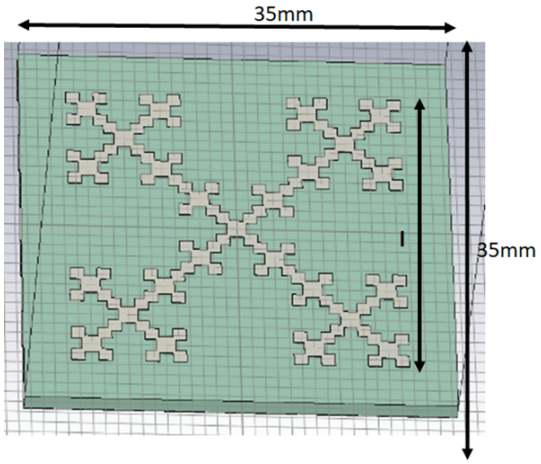

Figure 2.12: Third iteration of Minkowski fractal

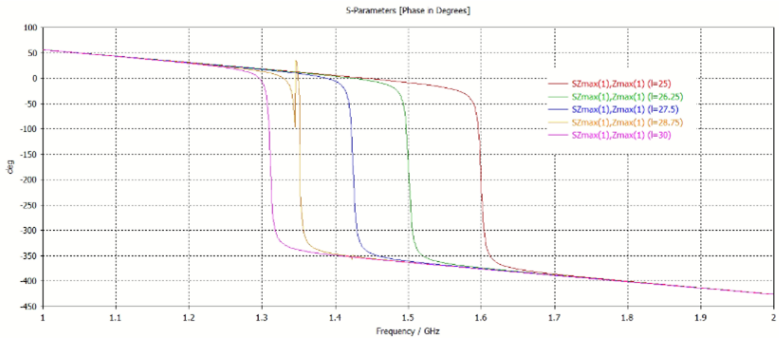

Figure 2.13: Phase of S_{11} for different patch lengths (in mm) at frequency = 1.5 GHz.

2.2 Synthesis of Reflectarray

In the next step, the fractals corresponding to 0˚ and 180˚ phases are used to achieve 1-bit discretization of the reflectarray. The idea is to generate a reflecting surface such that the fractals corresponding to 0˚ and 180˚ phase change, placed in a certain order, generate a beam in the intended direction when illuminated by a feed antenna as shown in Figure 1.1. Since each cell has a periodicity of 35mm, 16×16 array of unit cells will generate a RA of 560mm×560mm. For a 6U CubeSat, the RA can be realized by deploying panels placed on 3 faces of the CubeSat as in ISARA [4].

The Equation (1.4) gives the phase change corresponding to the i_{th} unit cell in the reflector. However, the equation provides a continuous phase distribution of the 256 unit cells. Practical limitations of resolution and fabrication complexity require the continuous phase distribution to be

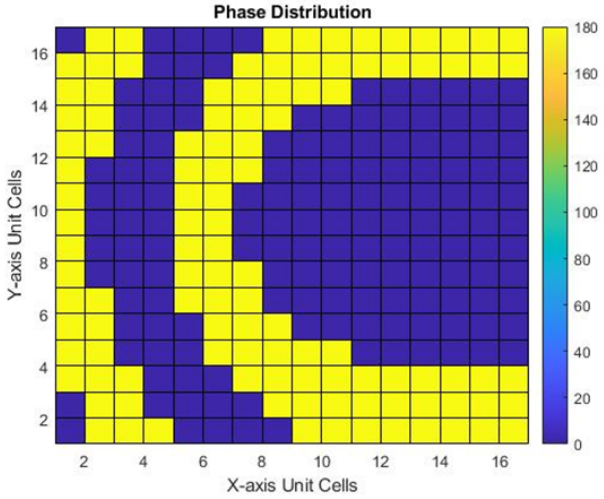

Figure 2.14: Quantized phase profile of RA.

discretized. Since phase change achieved in the unit cell is from 0˚ to 180˚, the continuous phase of 360˚ is discretized into 2 distinct phases with a phase change of 180˚.

The fractals corresponding to 0˚ and 180˚ are shown in Figure 2.15a and Figure 2.15b. These two fractals are used to generate the entire RA as per the phase discretization given in Figure 2.14.

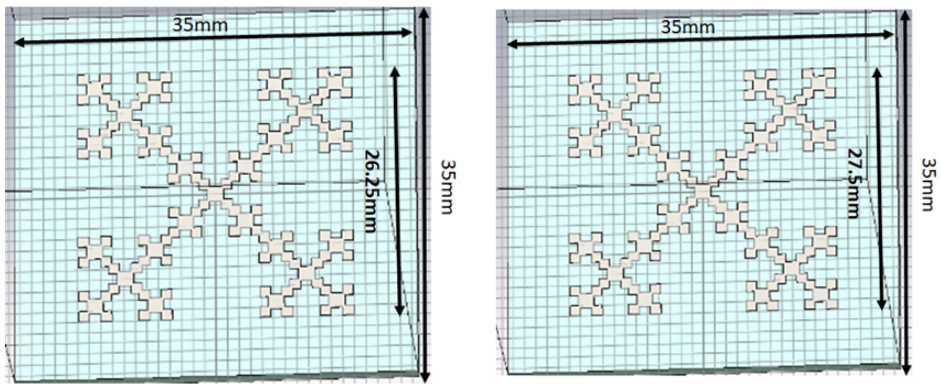

(a) **(b)**

Figure 2.15: (a.) 180˚ phase fractal (b.) 0˚ phase fractal.

The configuration of the unit cells in Figure 2.14 is specific to the distance from the feed antenna, which is 20cm, and the intended beam direction, which is 30˚. This phase profile has been generated using the mathematical expressions in [25] with the help of MATLAB code. The corresponding unit cell placement in the RA as in Figure 2.16 was automated with the help of python script in HFSS. Mr. Akhila Gowda assisted in the MATLAB coding, python scripting and HFSS modelling. He is a PhD student of Applied Electromagnetics Lab, under supervision of Dr. Saptarshi Ghosh, Associate Professor in the Department of Electrical Engineering, IIT Indore The

complete RA structure of 256 cells is then imported into CST where further simulations are carried out for the entire RA system with the feed antenna.

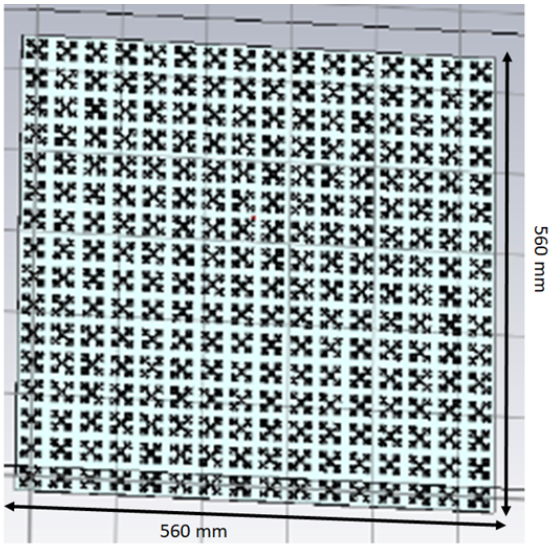

Figure 2.16: Designed RA.

2.3 Design of Feed Antenna

Initially, a directional planar antenna was selected. Since reflectarrays are usually fed with highly directional horn antennas, planar alternative for the same was investigated, which is an antipodal Vivaldi array. FR4 substrate of height 1.5mm has been chosen. The gain of the AVA array is shown in Figure 2.18. However, the dimensions of the array alone is 215mm×265mm as illustrated in Figure 2.17.

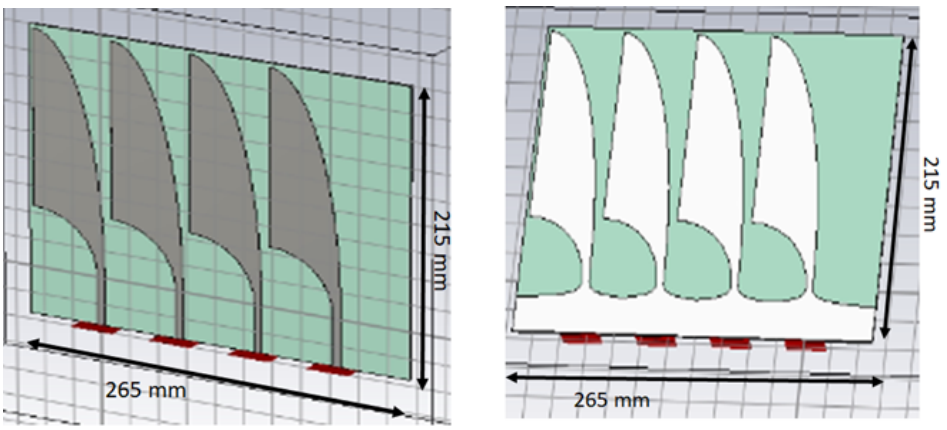

(a) top view **(b)** ground plane

Figure 2.17: Antipodal Vivaldi Antenna Array

The array together with a power divider would be of substantial size. It would be troublesome to make this feed antenna deployable on a CubeSat together with the RA which is of equivalent size. The entire system would be too bulky for a CubeSat. Thus, a simpler planar antenna, a patch array antenna, was chosen which is to be integrated as the feed of the RA system. A patch antenna has low gain and directivity. Thus a 2×2 array of the same would improve the gain and directivity without increasing the dimensions substantially.

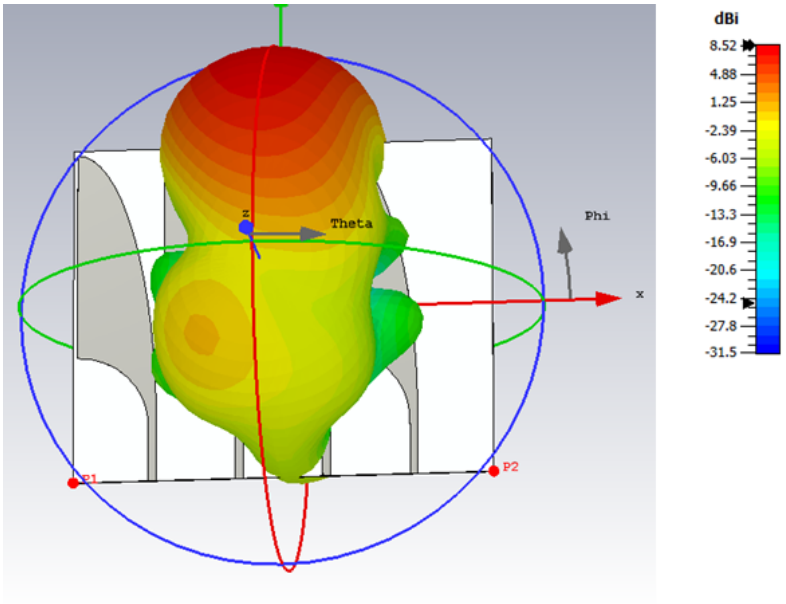

Figure 2.18: Gain of AVA array

2.3.1 Probe-fed single patch

In [4] the feed antenna is chosen to be a patch array to accommodate the entire system on the CubeSat. Similarly, a planar patch array is to be designed as feed for this RA system. The first step is to design a resonant patch at 1.5 GHz. The substrate selected is FR4. Its dielectric constant is 4.3, thus the size for the resonant patch will be smaller resulting in compact array. The patch is probe-fed with inner diameter 1.2mm and outer diameter 4mm. The geometry is illustrated in Figure 2.19. Probe feeding design is selected for its compactness. It has a gain of 6.21dBi as seen in Figure 2.20. The S_{11} in Figure 2.21, is -29dB at 1.5 GHz. The square patch is of length 47mm. The length of the square ground is 94mm.

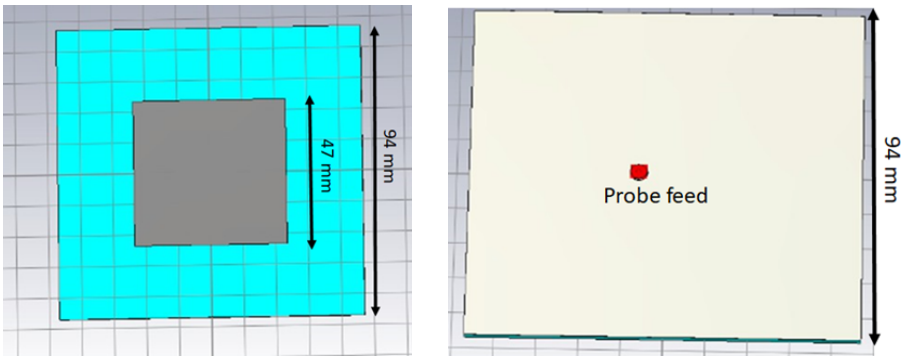

(a) top view **(b)** Bottom view

Figure 2.19: Probe-fed single patch

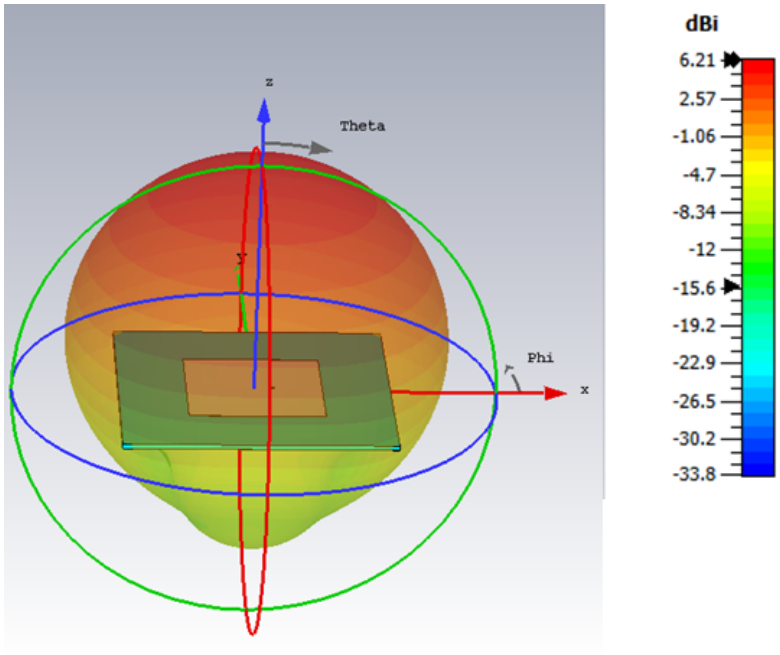

Figure 2.20: Gain of single patch

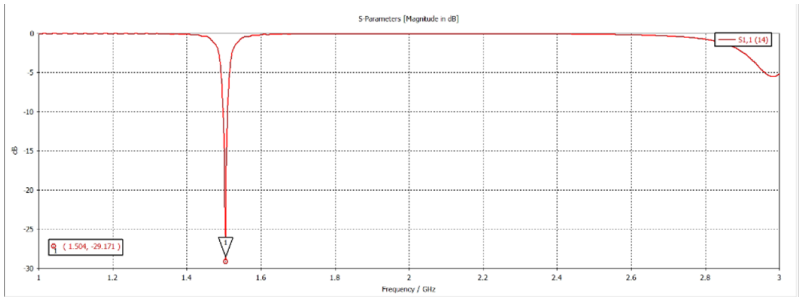

Figure 2.21: S_{11} of single patch

2.3.2 2×2 patch array with corporate feed

The resonant patch is now used to form 2×2 array. This will improve the directivity and gain for the antenna. Four square patches of length 47mm are designed on FR4 of height 1.58mm with a continuous ground at the bottom. The overall dimension of the array is 200mm×200mm as seen in Figure 2.22.

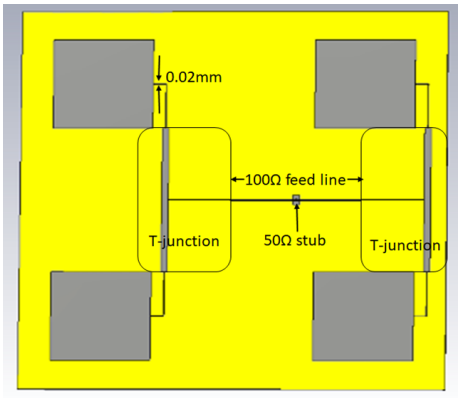

Figure 2.22: 2×2 patch array with corporate feed

Corporate feeding network is used so as to make the array compact. Feed line coming out of each patch has width corresponding to the edge impedance of the patches. Due to practical purpose of fabrication, instead of the exact required width of the microstrip line, the width has been so chosen such that the losses incurred due to mismatch is minimal. The feed lines from the two patches in each row are then matched to the 100Ω central line via T-junction. The probe feed is attached to the center of this 100Ω line through a 50Ω stub.

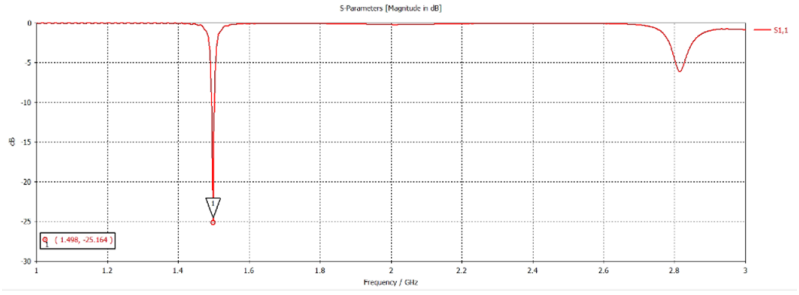

Figure 2.23: S_{11} of the feed array

This particular array along with the feed design has shown 11dBi gain shown in Figure 2.24. Figure 2.23 shows S_{11} to be -25dB. This particular design has been achieved with the assistance of Dr. Rinkee Chopra, Assistant Professor in the Department of Electrical Engineering, IIT Indore.

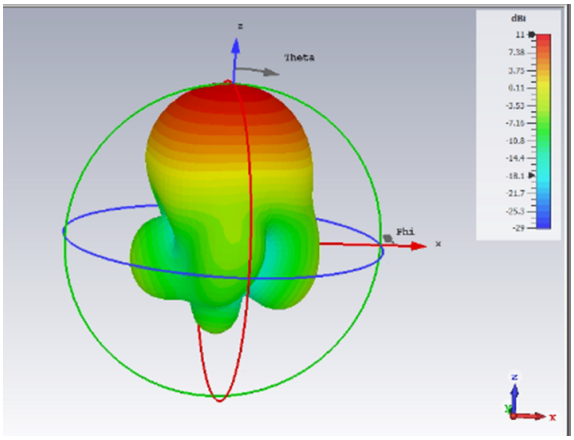

Figure 2.24: Gain of the feed array

2.4 RA With Feed

The concept of RA is that it will transform the spherical wave front radiated from the feed into plane wave. Thus, closer the distance from the feed, better the chance of gain enhancement. To avoid feed overload, the starting distance of trials for optimization was 50mm. Gradually, the distance from the feed had to be increased and the number of cells of the RA also had to be increased from 9×9 array to 16×16 to overcome feed blockage. This simulation is carried out in CST studio 2019 in a computer with 95 GB RAM. Some optimization attempts required higher computational facility which compelled a server to be used from AEM lab with the help of Mr. Akhila Gowda.

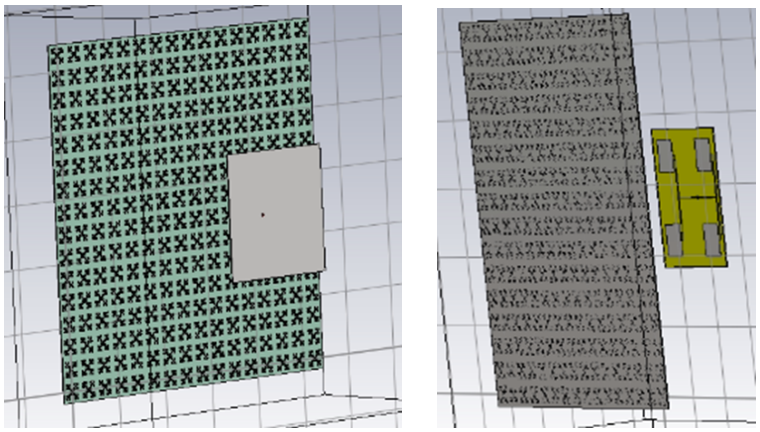

(a) top view **(b)** side view

Figure 2.25: RA with feed antenna

In the final step, the synthesized 1-bit discretized RA is placed at a distance of 200mm from the center of the feed patch array. The RA is designed for this particular distance and 30˚ beam bending. The RA in the Figure 2.25 is made up of 16×16 unit cells, each of periodicity 35mm.

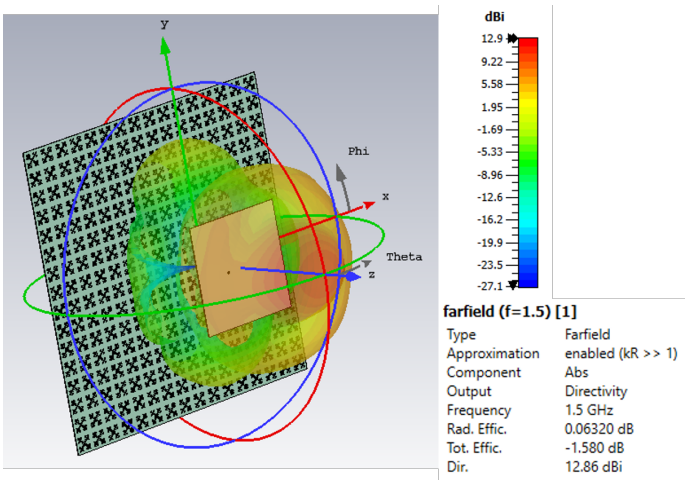

Figure 2.26: Gain of the RA system

The feed antenna is a 2×2 patch array with corporate feed and port at the probe feeding face. The simulation result shows 12.9 dBi gain in Figure 2.26.

2.5 Results And Discussion

2.5.1 Unit Cell For Reflectarray

The single-layered unit cell for the L-band reflectarray has been designed as discussed in Chapter 3 on FR4 substrate with thickness 1.524mm. Its periodicity is 35mm×35mm. It is a 3rd iteration of the Minkowski fractal patch. The phase range that has been achieved by changing the overall patch length from 25mm to 26.25mm (approx.) is 0˚ to -180˚. Thus, the reflectarray can be designed with varying patches within the said range to collimate the radio waves in the direction of the feed antenna. Hence, phase tuning is achieved with the aid of miniaturization using fractal geometry as shown in Figure 2.27.

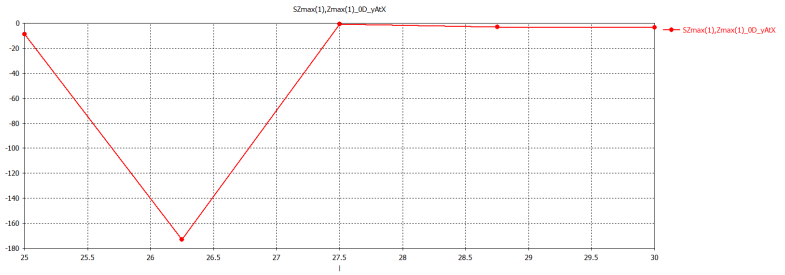

Figure 2.27: Phase of S_{11} for different patch lengths (in mm) at frequency = 1.5 GHz.

2.5.2 Reflectarray

The unit cell discussed above is used to form the entire reflectarray with 1-bit discretization of the analog phase distribution. The fractals corresponding to 0˚ and 180˚ are of length 27.5mm and 26.25mm respectively. These are used to produce the phase distribution as shown in Figure 2.28 computed with the help of MATLAB for a distance of 200mm from the feed. The MATLAB code used, realizes the Equation (1.4). The RA synthesized is made up of 16×16 array of unit cells, each of periodicity 35mm. The overall dimension of the RA is 560mm×560mm shown in Figure 2.29.

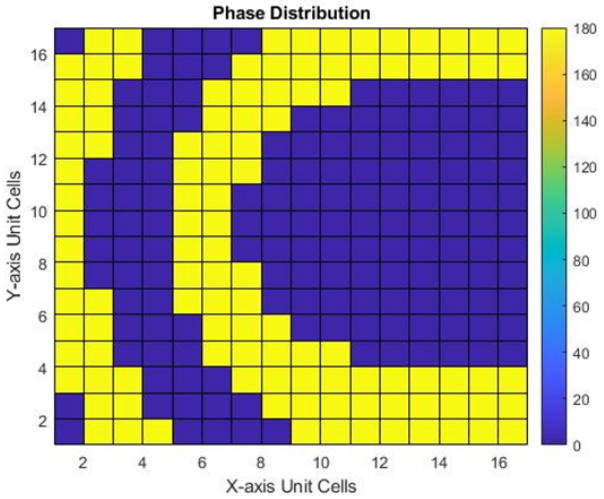

Figure 2.28: Phase distribution of the RA

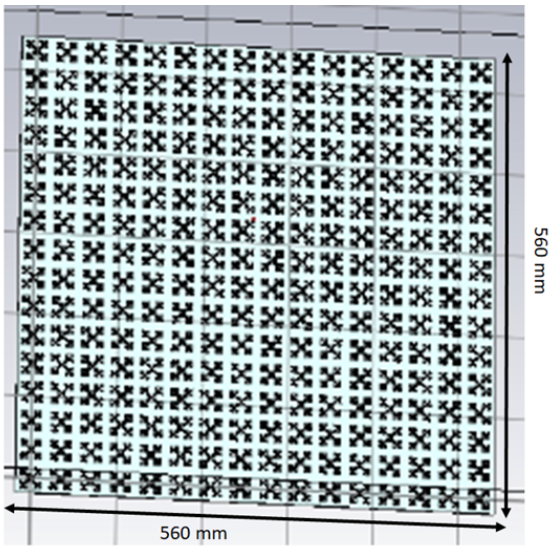

Figure 2.29: Designed RA

2.5.3 Feed Antenna

The feed antenna is a 2×2 patch array with corporate feed. It is designed on FR4 substrate with height 1.58mm. The design is optimized to obtain a gain of 11dBi at 1.5 GHz as seen in Figure 2.30. S_{11} obtained is -25dB illustrated in Figure 2.31.

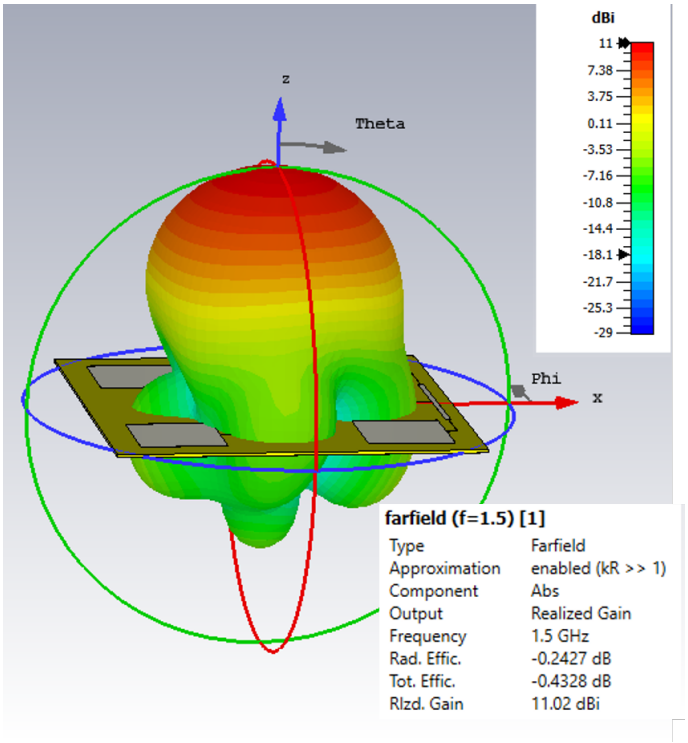

Figure 2.30: Gain of patch array

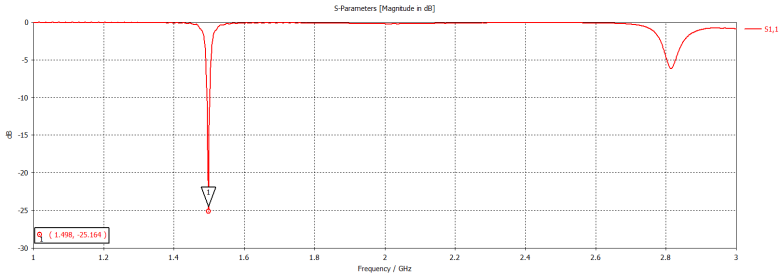

Figure 2.31: S_{11} of patch array

2.5.4 RA With Feed

The synthesized 1-bit discretized RA is placed at a distance of 200mm from the center of the feed patch array. The RA is computed for this particular distance and 30˚ beam bending. It is made up of 16×16 unit cells, each of periodicity 35mm. The feed antenna is a 2×2 patch array with

corporate feed. The simulation result in Figure 2.32 shows 12.9 dBi gain. Thus the reflectarray has increased the gain of the feed antenna by 1.9 dBi. The main lobe direction is, however, at 0˚ theta.

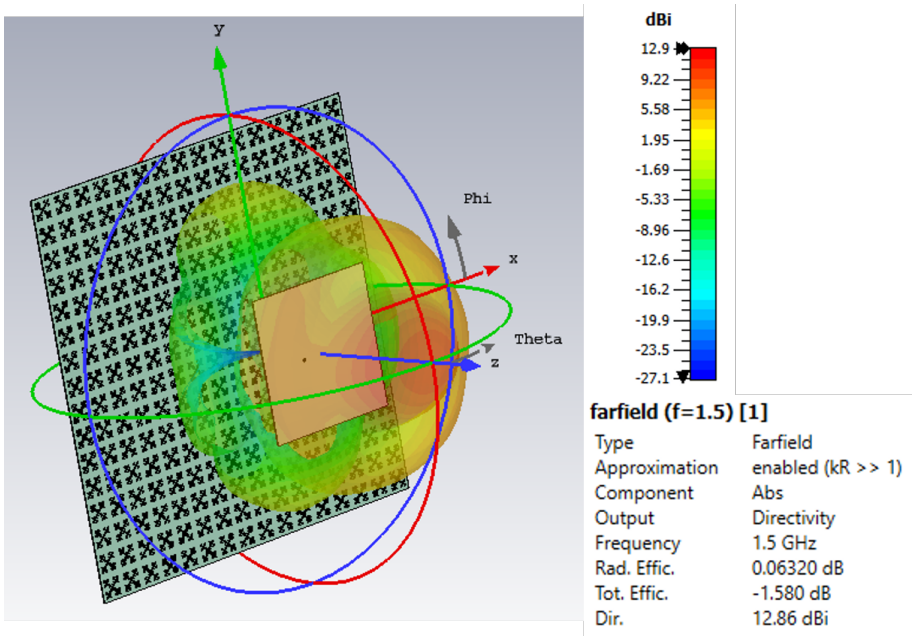

Figure 2.32: Gain of the RA system

Chapter 3

Arctic RFI Survey

RFI is an important aspect of radio astronomy. A precursor to CubeSat application can be an aerial RFI survey in the pristine radio-silent Arctic region using the reflectarray. Understanding and interpretation of the RFI data will, in turn, help in the betterment of the instrumentation, that is, the antenna. Radio telescopes have been deployed in the polar regions of the Arctic and Antarctica due to their unique environment as one of the world's most radio-silent zones. The logistical requirements for conducting radio astronomy experiments can be fulfilled by the research stations present on the poles. However, Antarctica being more remote, the Himadri Research Station in Svalbard presents itself as a more suitable site for studying faint cosmic signals. The Himadri Research Station in Svalbard is remote and has a sparse human population which significantly reduces the likelihood of terrestrial radio-frequency interference (RFI), making it an ideal lo- cation for sensitive radio observations. This research can contribute to our understanding of space weather and its effects on communication systems, satellite operations, and even climate.

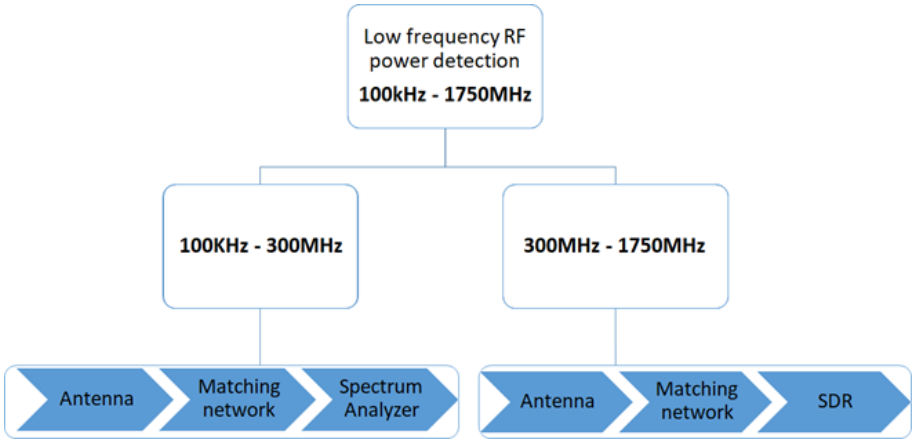

Figure 3.1: Flowchart of RFI detection.

The RFI detection approach for this experiment is shown in Figure 3.1. Antennas, connected to a matching network, were used to record the detected RFI in the 100 kHz to 300 MHz range using a Spectrum Analyzer. For the 300 MHz to 1750 MHz range, antennas with matching networks were employed to capture the detected power levels using a software-defined radio (SDR).

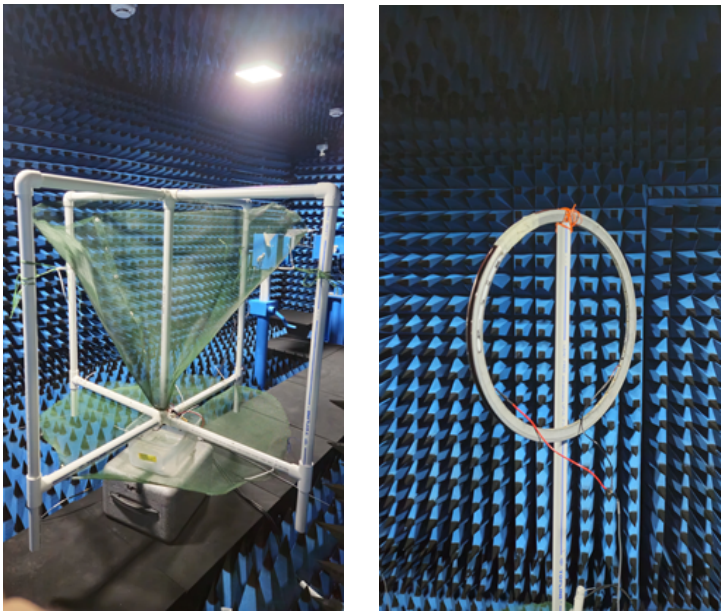

(a) Conical monopole antenna. **(b)** Loop antenna.

Figure 3.2: Antennas used for RFI detection.

Three types of antennas were employed: conical monopole, loop, and log-periodic dipole array (LPDA). The loop antenna, made from a 10-meter length of 8-gauge copper wire wound around a 26-inch cycle rim, was tuned for resonance. The conical monopole antenna used a mesh framework wrapped around PVC pipes for structural support. Figure 3.2 shows the in-house built antennas described above. The model for simulation of the discone is illustrated in Figure 3.3 and its parameters are described in Table 3.1.

Params	In cm
h	120
gap	10
Dia	754

Table 3.1: Parameters of discone

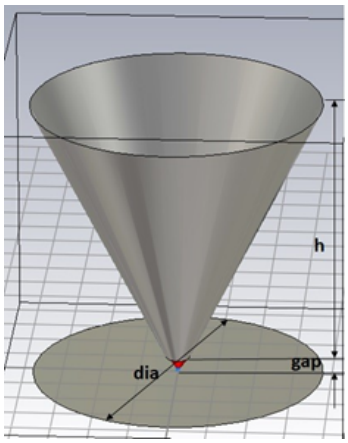

Figure 3.3: Design of Loop antenna

3.1 Results of Arctic RFI

At Himadri Station, antennas with various matching networks were deployed to monitor ambient RFI levels. The power levels recorded across the 100 kHz to 1750 MHz band were compiled to create Figure 3.4 and Figure 3.6, which depict the detected RFI across the frequency spectrum. In Figure 3.4, peaks in the 80-110 MHz range correspond to FM broadcasts, with additional peaks identified at 200.304 MHz and 209.13 MHz. The 800 MHz peak in Figure 3.6 represents radio emissions within the GSM band, while the high-power levels between 400-600 MHz are attributed to TV broadcasts. Figure 3.5 shows readings still affected by the RF amplifier and SDR responses. Further data processing in Figure 3.6 removes these effects by subtracting the S_{21} response of the RF amplifier and the SDR response.

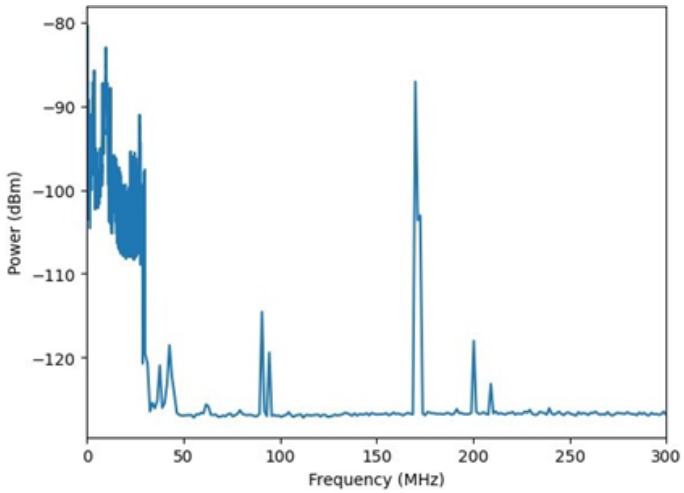

Figure 3.4: RFI survey reading, performed on June 19, 2024, combining data from Loop and Conical Monopole antennas.

The results show that the Arctic is exceptionally clear of terrestrial RFI as also presented in [15]. Below 50 MHz, RFI detected is below -80dBm in the Himadri Station. Himadri Station exhibits RFI, seen in Figure 3.7, comparable with [18] depicted in Figure 3.8 in the Arctic summers when the ionospheric plasma cut-off is higher than the typical cut- off frequencies. Therefore, the Himadri Station stands as a promising location for low-frequency radio astronomy observations, as it is particularly free from RFI in the 100 kHz to 1750 MHz frequency range. This is a continuing experiment in the Arctic.

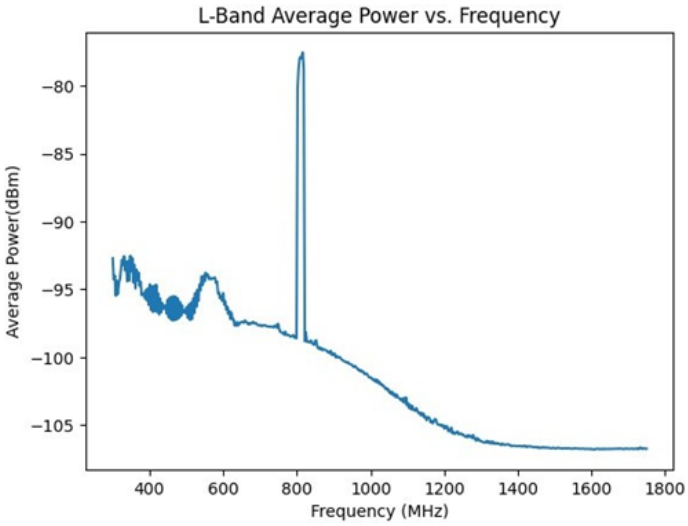

Figure 3.5: RFI survey reading, performed on Jun 19, 2024 in L-band generated by averaging four hours' data.

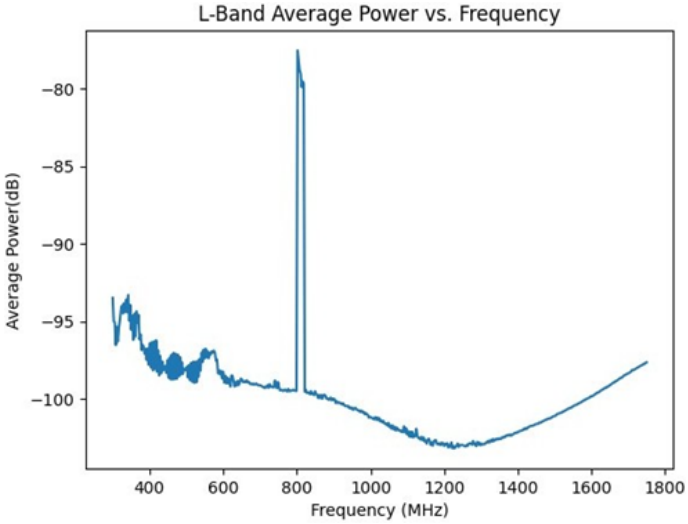

Figure 3.6: RFI survey reading in L-band, performed on Jun 19, 2024 after removing power amplifier's response.

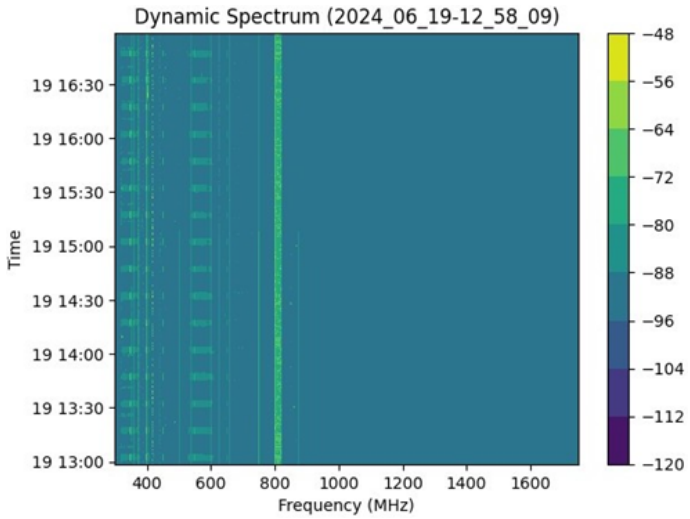

Figure 3.7: Dynamic spectrum of data recorded on June 19, 2024.

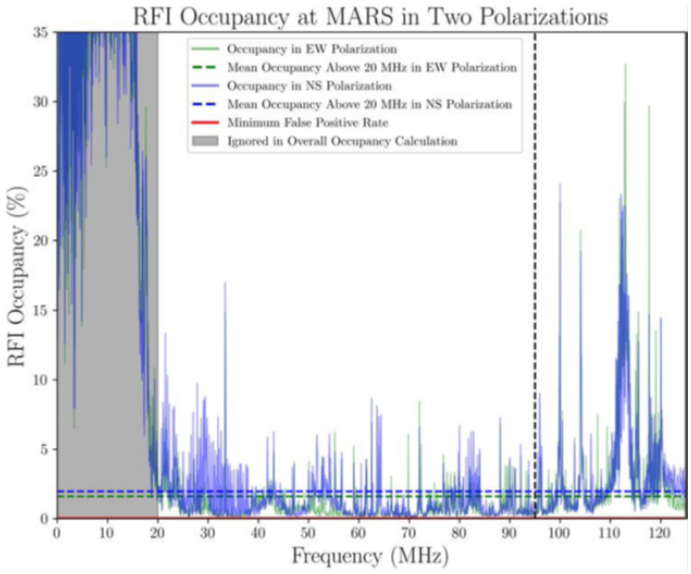

Figure 3.8: RFI Occupancy in McGill Arctic Research Station survey [15]

Chapter 4

Conclusions And Scope For Future Work

4.1 Conclusions

4.1.1 Reflectarray Antenna

In this thesis, the design and application of reflectarray antennas for CubeSat missions operating in the L-band have been explored, with a particular focus on space-based radio astronomy. The research presents miniaturizing reflectarray unit cells to meet the size requirements for Cube- Sats. Through the exploration of fractal geometries for element miniaturization and phase agility, the thesis highlights a novel approach to optimizing the size and performance of L-band reflectarray antennas.

The miniaturized unit cells are used to make a reflectarray with 16×16 array of unit cells and an overall dimension of 560mm×560mm. The continuous phase distribution has been transformed to 1-bit discretization with the help of the fractals corresponding to 0˚ and 180˚ phase change. This RA can be accommodated in a CubeSat in panels as in ISARA [4].

The feed antenna designed is a 2×2 patch array with corporate feed to accommodate the entire RA system in a CubeSat. The gain achieved by this structure is 11dBi at 1.5GHz, considering lossless substrate FR4 of height 1.58mm. This feed is placed at a distance of 200mm from the RA. The RA has been generated by coding the Equation (1.4) for this particular distance of 200mm and a beam bending of 30˚. The result shows that the overall gain of the entire RA system is 12.9dBi. The gain improvement from the feed due to the presence of the reflectarray is 1.9dBi. However, the beam bending has not been achieved. The main challenge for this research has been the low frequency of 1.5GHz which has posed a huge computational obstacle. The research has

been carried out with CST studio 2019 in a computer with 95GB RAM. But the low frequency of operation requires more computational facility for further optimization and improvement of the reflectarray which was not available for perusal. Another issue of the outcome is the fact that the reflectarray and the feed antenna are of comparable sizes. Thus the feed has a blocking effect on the reflecting surface. Offset feeding can be explored however, the complexity of the arrangement of the RA system for space deployability will increase in this case. Also, the unit cell can be further optimized to achieve higher range of phase tuning, thus facilitating higher order of discretization in place of 1-bit discretization. This will, in turn, improve the phase distribution of the reflectarray and result in better aligning the outcome with the expected result as per the Equation (1.4).

4.1.2 Arctic RFI Survey

RFI study in the Arctic was conducted to gain a perspective of the use of antennas for radio astronomical purposes.The experiment conducted in the Arctic studies the RF emissions in the environment. Low-frequency antennas, such as loop, horn, conical monopole, and LPDA, were used to record data for this purpose. The plotted data show power emission in the FM broadcasting band (80-110 MHz), TV broad- casting band (400-600 MHz), and GSM band (800 MHz) are lower than other sites[4], [6] and [8]. The results show Himadri Station as an ideal site for low frequency radio astronomy observations like the Cosmic Dawn signals as most of the bands between 100 kHz – 1750 MHz is significantly clear of terrestrial RFI. Additionally, the study explores the radio-silent Himadri Research Station as a potential site for future reflectarray deployments.

4.2 Future Work

The proposed work presents a reflectarray at 1.5GHz together with a feed patch array antenna to be deployed in a CubeSat with gain 12.9dBi. Although optimization of the size and performance has been explored in this thesis, further scope of research can be considered in the following areas:

- Improving phase tuning range for the unit cell.
- Offset feed for the reflectarray.
- Space deployability of the entire system in the CubeSat.

Chapter A

APPENDIX-A

Some other geometries explored are as follows:

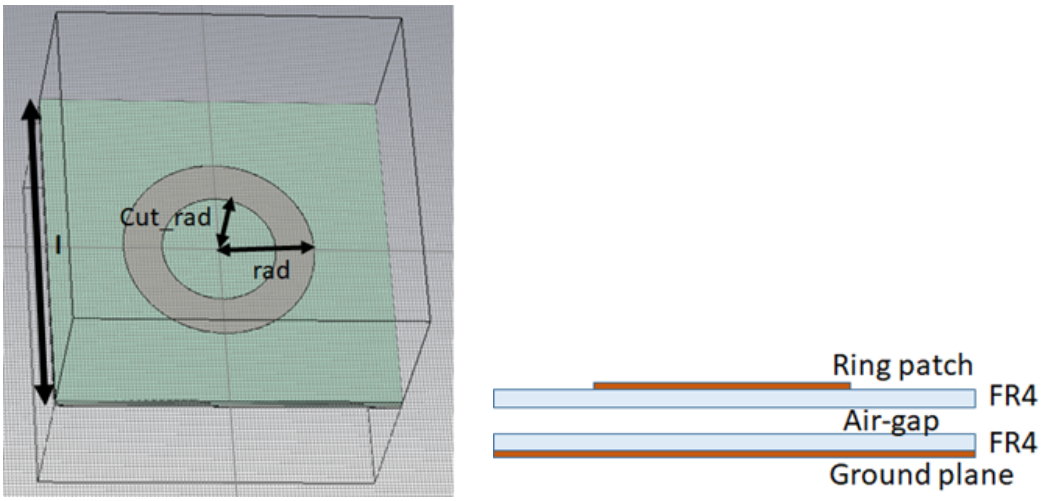

(a) **(b)**

Figure A.1: (a.)Ring Patch (b.)Configuration of the substrates and air-gap of the unit cell.

Parameter	Dimension (mm)
Length of the square unit cell (l)	90
Radius of the outer circle of the patch (rad)	25.2
Radius of the inner circle (cut_rad)	5-15 (varied)
FR4 height	1.5
Airgap	2

Figure A.2: Parameters of the design with dimensions.

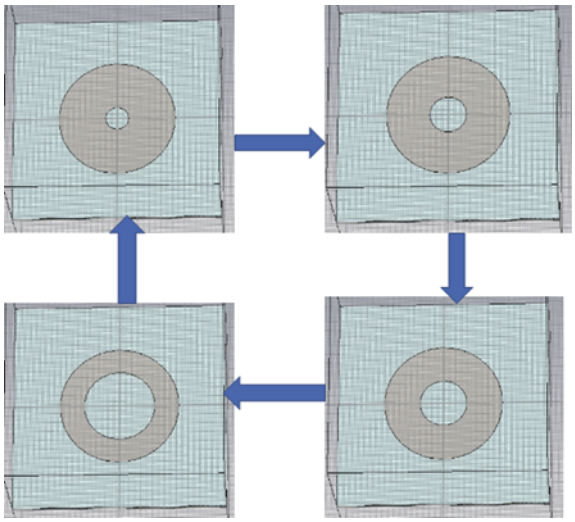

Figure A.3: 3 Variation of the ring patch for different inner radius, outer radius = 25.2mm.

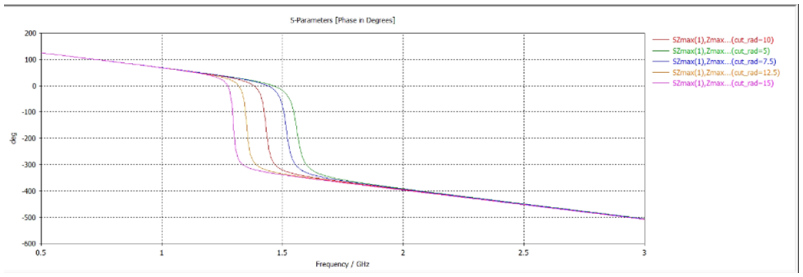

Figure A.4: Phase of S11 for different inner radius (cut$_rad$), $outerradius = 25.2mm$.

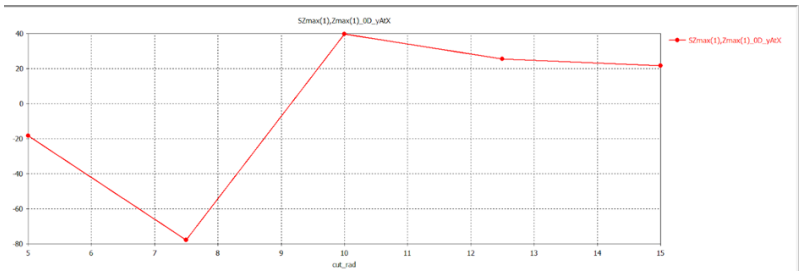

Figure A.5: 5 Phase of S11 for different inner radius at frequency = 1.4GHz.

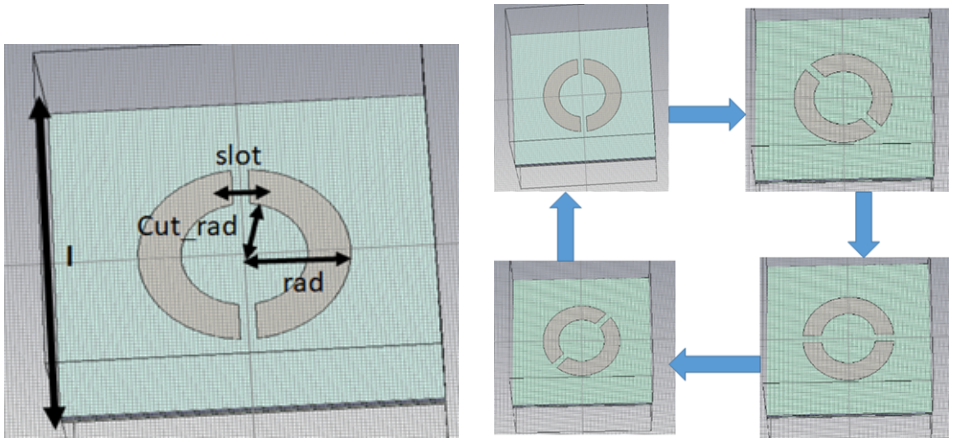

(a) **(b)**

Figure A.6: (a.)Slotted ring patch geometry. (b.) Slotted ring parametric study by rotation of the patch

Parameter	Dimension (mm)
Length of the square unit cell (l)	90
Radius of the outer circle of the patch (rad)	25.2
Radius of the inner circle (cut_rad)	15
FR4 height	1.5
Airgap	2
Slot	2

Figure A.7: Parameters of the design with dimensions.

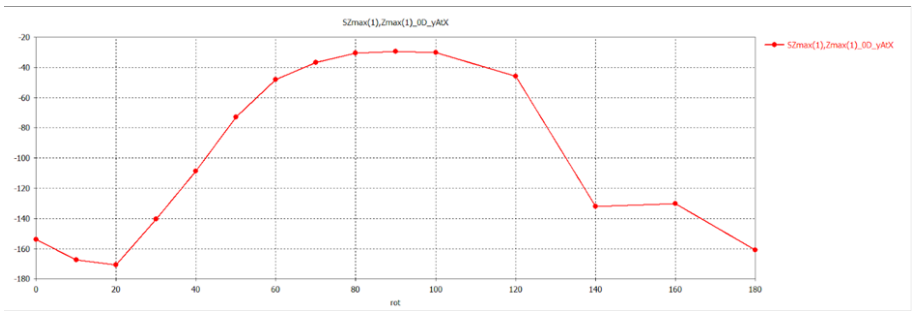

Figure A.8: Phase of S11 for different rotating angles (in degrees) at frequency = 1.4GHz.

Bibliography

[1] Carrasco, Eduardo, Jose A. Encinar, and Y. Rahmat-Samii. ”Reflectarray antennas: A review.” Forum for Electromagnetic Research Methods and Application Technologies (FERMAT). Vol. 16. 2016.

[2] M. H. Dahri, M. H. Jamaluddin, M. I. Abbasi and M. R. Kamarudin, ”A Review of Wideband Reflectarray Antennas for 5G Communication Systems,” in IEEE Access, vol. 5, pp. 17803-17815, 2017, doi: 10.1109/ACCESS.2017.2747844.

[3] J. Huang, ”The development of inflatable array antennas,” IEEE Antennas Propag. Mag., vol. 43, no. 4, pp. 44-50, Aug. 2001.

[4] R. E. Hodges, D. J. Hoppe, M. J. Radway and N. E. Chahat, ”Novel deployable reflectarray antennas for CubeSat communications,” 2015 IEEE MTT-S International Microwave Symposium, Phoenix, AZ, USA, 2015, pp. 1-4, doi: 10.1109/MWSYM.2015.7167153.

[5] X. Zhu, S. Xu and F. Yang, ”Design of an L-band reflectarray antenna for BeiDou satellite applications,” 2014 International Symposium on Antennas and Propagation Conference Proceedings, Kaohsiung, Taiwan, 2014, pp. 297-298, doi: 10.1109/ISANP.2014.7026648.

[6] T. Smith, U. Gothelf, O. S. Kim and O. Breinbjerg, ”An FSS-Backed 20/30 GHz Circularly Polarized reflectarray for a Shared Aperture L- and Ka-Band Satellite Communication Antenna,” IEEE Transactions on Antennas and Propagation, vol. 62, no. 2, pp. 661-668, Feb. 2014, doi: 10.1109/TAP.2013.2292692.

[7] M. E. Bialkowski and K. H. Sayidmarie, ”Investigations Into Phase Characteristics of a Single-Layer Reflectarray Employing Patch or Ring Elements of Variable Size,” in IEEE Transactions on Antennas and Propagation, vol. 56, no. 11, pp. 3366-3372, Nov. 2008, doi: 10.1109/TAP.2008.2005470.

[8] D. M. Pozar and T. A. Metzler, ”Analysis of a reflectarray antenna using microstrip patches of variable size,” Electron. Lett., vol. 29, no. 8, pp. 657-658, Apr. 1993.

[9] F.-C. E. Tsai and M. E. Bialkowski, ”Designing a 161-element Ku-band microstrip reflectarray of variable size patches using an equivalent unitcell waveguide approach,” IEEE Trans. Antennas Propag., vol. 51, no. 10, pp. 2953-2962, Oct. 2003.

[10] M. Bozzi, S. Germani and L. Perregrini, ”Performance comparison of different element shapes used in printed reflectarrays,” Proc. IEEE Antennas Wireless Propag. Lett., vol. 2, pp. 219-222, 2003.

[11] N. Misran, R. Cahill and V. Fusco, ”Design optimisation of ring elements for broadband reflectarray antennas,” Inst. Elect. Eng. Proc. Microw. Antennas Propag., vol. 150, no. 6, pp. 440-444, Dec. 2003.

[12] M. R. Chaharmir, J. Shaker, M. Cuhaci and A. Ittipiboon, ”Broadband reflectarray antenna with double cross loops,” Electron. Lett., vol. 42, no. 2, pp. 65-66, Jan. 2006.

[13] S. Costanzo and F. Venneri, ”Miniaturized Fractal Reflectarray Element Using Fixed-Size Patch,” in IEEE Antennas and Wireless Propagation Letters, vol. 13, pp. 1437-1440, 2014, doi: 10.1109/LAWP.2014.2341032.

[14] F. Zubir and M. K. A. Rahim, ”Simulated fractals shape for unit cell reflectarray,” 2009 Asia Pacific Microwave Conference, Singapore, 2009, pp. 583-586, doi: 10.1109/APMC.2009.5384161.

[15] T. Dyson, H. C. Chiang, et al., “Radio-frequency interference at the McGill Arctic Research Station,” Journal of Astronomical Instrumentation, vol. 10, no. 2, p. 2150007, 2021.

[16] T. Dyson, H. C. Chiang, et al., “The array of long baseline antennas for taking radio observations from the sub-antarctic,” Journal of Astronomical Instrumentation, vol. 9, no. 4, p. 2050019, 2020.

[17] J. D. Bowman, A. E. E. Rogers, R. A. Monsalve, T. J. Mozdzen, and N. Mahesh, “An absorption profile centred at 78 megahertz in the sky-averaged spectrum,” Nature, vol. 555, no. 7694, pp. 67–70, Mar. 2018.

[18] C. DiLullo, G. B. Taylor, and J. Dowell, “Using the long wavelength array to search for cosmic dawn,” Journal of Astronomical Instrumentation, vol. 9, no. 2, p. 2050008, 2020.

[19] J. Hickish, Z. Abdurashidova, Z. Ali, et al., “A decade of developing radio-astronomy instrumentation using CASPER open-source technology,” Journal of Astronomical Instrumentation, vol. 5, no. 4, p. 1641001, 2016.

[20] B. C. Hicks, N. Paravastu-Dalal, K. P. Stewart, et al., “A wide-band, active antenna system for long wavelength radio astronomy,” Publications of the Astronomical Society of the Pacific, vol. 124, no. 920, p. 1090, Sep. 2012.

[21] N. Bassett, D. Rapetti, K. Tauscher, et al., “Lost horizon: quantifying the effect of local topography on global 21 cm cosmology data analysis,” The Astrophysical Journal, vol. 923, no. 1, p. 33, Dec. 2021.

[22] L. Philip, Z. Abdurashidova, H. C. Chiang, et al., “Probing radio intensity at high-Z from Marion: 2017 instrument,” Journal of Astronomical Instrumentation, vol. 8, no. 2, p. 1950004, 2019.

[23] S. Singh, R. Subrahmanyan, N. U. Shankar, et al., “SARAS 2 constraints on global 21 cm signals from the epoch of reionization,” The Astrophysical Journal, vol. 858, no. 1, p. 54, May 2018.

[24] S. S. Kristensen, S. S. Søbjærg, J. E. Balling, N. Skou, “Arctic sea ice monitored at L-band: initial results and RFI findings,” in 2021 IEEE International Geoscience and Remote Sensing Symposium IGARSS, p. 1835–1838, 2021.

[25] Nayeri, Payam & Elsherbeni, Atef. (2018). Reflectarray Antennas: Theory, Designs, and Applications. 10.1002/9781118846728.